Hindawi
International Journal of Energy Research
Volume 2024, Article ID 2548688, 14 pages
https://doi.org/10.1155/2024/2548688

Research Article

A Concept of Online Refueling TRISO-Fueled and Salt-Cooled Reactor

Xiaoyong Feng and Hyun Chul Lee

School of Mechanical Engineering, Pusan National University, 2, Busandaehak-ro 63beon-gil, Geumjeong-gu, Busan 46241, Republic of Korea

Correspondence should be addressed to Hyun Chul Lee; hyunchul.lee@pusan.ac.kr

Received 12 September 2023; Revised 12 March 2024; Accepted 28 March 2024; Published 16 April 2024

Academic Editor: Ozguer Omer Ersin

This paper introduces a novel concept of a TRISO-fueled salt-cooled reactor (TFSCR). The core contains circulating pipes filled with molten salt carrying TRISO particles. The reactor achieves online refueling by slowly circulating the molten salt through the pipeline. The reactor utilizes the same molten salt as the coolant and graphite as the moderator. The reactor design has the characteristics of safety, economy, and nonproliferation. TRISO particles exhibit greater resistance to neutron irradiation, corrosion, oxidation, and high temperatures compared to conventional fuels. A molten salt-cooled reactor can also operate at higher temperatures, consequently enhancing power generation efficiency. Furthermore, lower operating pressures can mitigate the risk of significant damages and loss of coolant caused by accidents, thereby enhancing reactor safety. This paper presents the basic nuclear design of TFSCR under the assumptions concerning the average fuel power density, the volumetric core power density, and the core temperature. At the same time, the feasibility of online refueling and long-life operation was evaluated by fuel burnup calculation.

1. Introduction

Molten salt reactors (MSRs) are a fourth-generation reactor design that utilizes molten salt as both liquid fuel and coolant, setting them apart from conventional reactors. Unlike light water reactors (LWRs), MSRs operate at near-atmospheric pressure and can reach operating temperatures as high as 700-750°C [1]. The use of molten salt as a coolant provides notable advantages, including its exceptional heat capacity and higher boiling point [1, 2]. By eliminating the requirement for high-pressure operation and water cooling, MSRs effectively minimize the risk of loss of coolant accident (LOCA) and the related incidents, such as hydrogen explosions [2, 3].

Some variants of MSRs, known as Fluoride-salt-cooled High-temperature Reactors (FHRs), utilize a solid form of fuel and molten salt coolant. Table 1 lists the basic information of some MSRs and FHRs as well as APR1400, a typical pressurized water reactor (PWR). [4–10].

Liquid fuel systems offer several advantages over solid fuel element systems, including a larger negative temperature coefficient of reactivity. Furthermore, liquid fuel systems can be combined with online fuel processing technology, ensuring the sustainability of the core. In the event of reactor failure, the fuel salt can be drained into a subcritical storage tank, providing a potentially safer approach to nuclear energy. However, the design of liquid fuel cores does pose challenges. A major concern is the absence of cladding around the fuel, which exposes the structural materials of the core to significant radiological contamination. Another issue is the effective separation of the fuel from the molten salt after shutdown.

FHRs are similar to the High-Temperature Gas-cooled Reactor (HTGR) design and can be categorized into three types [2, 11]: the prismatic block reactor design, the pebble bed design, and the recently proposed Advanced Gas-cooled Reactor (AGR) type design. It is worth noting that the prismatic block reactor design, such as the Advanced

Table 1: Key design parameters of some MSRs and FHRs.

Reactor design	Fuel form	Control rod	Thermal power (MWth)	Core inlet/exit temperatures (°C)	Fuel enrichment (wt%)	Discharge burnup of fuel (MWd/kg)	Coolant moderator	Average fuel power density (KW/kgU)	Average core power density (MW/m^3)
APR1400	Fuel assembly (UO_2)	Gd_2O_3	3983	290.6/323.9	^{235}U 4.65	46.5	H_2O H_2O	38.44	100.5
LFTR	Liquid fuel ($LiF\text{-}BeF_2\text{-}UF_4$)	B_4C	600	500/650	^{233}U 0.3	—	$LiF\text{-}BeF_2$ Graphite	—	—
MSR-FUJI	Liquid fuel ($LiF\text{-}BeF_2\text{-}ThF_4\text{-}UF_4$)	B_4C	450	565/704	^{233}U 0.24 Th 12.0 Pu or LEU	—	$LiF\text{-}BeF_2$ Graphite	—	5.5
MSTW	Liquid fuel (sodium-actinide fluoride)	B_4C	270	700/900	Th 93.0 U 3.5 Pu 3.5	250	$LiF\text{-}BeF_2$ Graphite	—	—
AHTR	Compact with TRISO	B_4C	2400	900/1000	^{235}U 10.36	—	$LiF\text{-}BeF_2$ Graphite		8.3
Smith	Compact with TRISO	B_4C	125	670/700	^{235}U 8.0	69	$LiF\text{-}BeF_2$ Graphite	—	9.4
Mk1 PB-FHR	Pebble with TRISO	B_4C	236	626/1371	^{235}U 19.9	180	$LiF\text{-}BeF_2$ Graphite	370	23

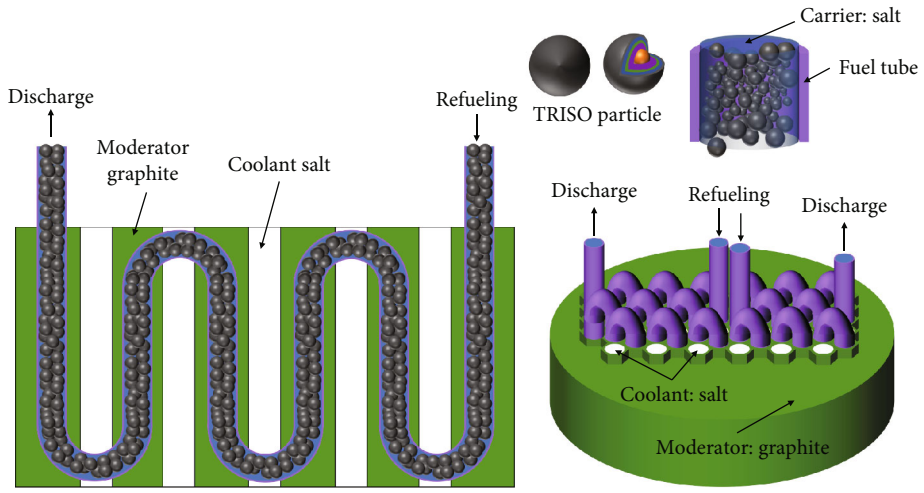

Figure 1: The reactor model diagram of TFSCR.

TRISO particle size parameters	
Outer pyrolytic carbon thickness	27 μm
Silicon carbide thickness	60 μm
Inner pyrolytic carbon thickness	35 μm
Porous carbon buffer thickness	120 μm
Fuel kernel radius	400 μm

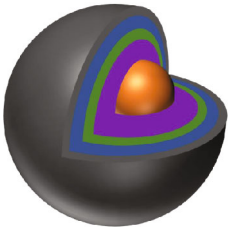

Outer pyrolytic carbon
Silicon carbide
Inner pyrolytic carbon
Porous carbon buffer
Fuel kernel [UO_2]

Figure 2: Schematic diagram of the TRISO particle structure.

High-Temperature Reactor (AHTR) [8], lacks the capability of online refueling and may exhibit a positive void coefficient. Moreover, an alternative approach, known as the Pebble-Bed Fluoride-salt-cooled High-temperature Reactor (PB-FHR) [10], allows online refueling and ensures a negative void coefficient. However, this design involves discharging spherical fuel elements from the core and processing them outside the core. As a result, nuclear fuel has to be removed from the reactor core for inspection before it can be returned, introducing radiation exposure issues. The recycled pebble is randomly located in the core, and therefore, the composition of the core is determined stochastically, not deterministically, which introduces an additional uncertainty in reactor operations.

To address the challenges in MSR and FHR design, this paper proposes the concept of a TRISO-fueled salt-cooled reactor (TFSCR) and a nuclear design of TFSCR. The TFSCR employs a core design which utilizes TRi-structural ISOtropic (TRISO) fuel particles as the fuel, graphite as the moderator, and molten salt as the coolant. In the TFSCR design, both the fuel and coolant are arranged in a hexagonal pattern, However, the TFSCR concept introduces interconnected U-shaped tubes in all fuel channels, allowing molten salt to act as a carrier for TRISO particles within the fuel tube. The same salt as the coolant salt is used as the carrier salt, but the role of the carrier salt is to transport the TRISO fuel particles very slowly from the inlet to the outlet of the fuel tube. This unique configuration enables online refueling, with molten salt gradually transporting fuel particles along the fuel channels. Fresh TRISO fuel enters through the inlet, while spent TRISO fuel is discharged from the outlet, and the fuel cycle is realized inside the core. Figure 1 illustrates the reactor model diagram.

The TFSCR proposed in this paper offers several advantages. By using molten salt as a coolant, it enables the acquisition of a high-temperature heat source from a nuclear reactor. This high-temperature heat source enhances the thermal efficiency of power generation and expands the range of applications of the heat source. Unlike liquid-fueled MSRs, the TFSCR does not have contamination issues in both normal operating conditions and transient scenarios. The fission products are effectively encapsulated within the TRISO particles as long as the temperature of TRISO particles remains below 1600°C [12, 13]. The use of TRISO fuel provides the advantage of enhancing nuclear nonproliferation and reducing the risk of nuclear weaponization. The latest study conducted accident experiments and simulation calculations for HTGR and LWR, revealing that TRISO particle-based high-temperature reactors can be flexibly optimized to effectively meet the requirements of both

Table 2: Physical properties of candidate coolants.

Material	Melting point (°C)	Normal boiling point (°C)	Density (ρ) (g/cm^3)	Heat capacity (C_p) (cal/g-°C)	Viscosity (μ) (cP)	Volume expansivity (β) (1/°C)	Thermal conductivity (k) (W/m-K)
Water	0	100	—	1.37	0.09	3.30*E*-03	0.54
LiF-BeF_2 (66-34)	460	1400	1.9384	0.577	5.6	2.52*E*-04	1
NaF-BeF_2 (57-43)	340	1400	2.0110	0.520	7	1.84*E*-04	0.87
NaF-ZrF_4 (57-43)	500	1350	1.9840	0.280	5.1	2.96*E*-04	0.49

Table 3: Coolant cooling capacity figures of merit (FOM).

Coolant	Turbulent forced convection	Heat exchanger area	Turbulent natural convection	Laminar natural convection
Water	0.20	13.0	4.8	0.63
LiF-BeF_2 (66-34)	0.70	21.5	13.9	10.12
NaF-BeF_2 (57-43)	1.98	37.4	14.7	7.90
NaF-ZrF_4 (57-43)	0.91	25.2	16.5	13.45

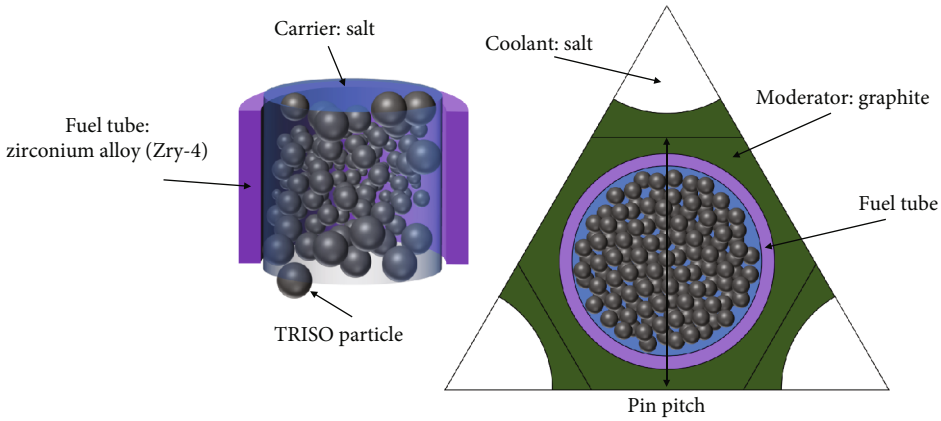

Figure 3: Unit cell model.

economy and safety [14–16]. Another benefit of the TFSCR is its online refueling capability, allowing the reactor to maintain a low excess reactivity and reducing the risk of reactivity-induced accidents. TRISO particles move in the pipeline, and the entire fuel cycle process is carried out inside the core. When an emergency occurs, control rods or fuel evacuation can be used to ensure safety.

2. Nuclear Design of TFSCR Core

The nuclear design of the TFSCR core was conducted based on the following assumptions: Considering the fluidity of TRISO particles, the packing fraction of TRISO particles in the fuel tube is assumed to be 50%, slightly lower than the theoretical maximum packing fraction of spheres in a cylinder, which is 64% [17]. The average volumetric power density and the average fuel power density are assumed to be approximately 8 W/cm^3 and 60 W/gU, respectively, which are similar to those of AHTR [8]. Considering the temperatures of other salt-based reactors, the fuel temperature, graphite temperature, and coolant temperature are assumed to be 1200 K, 1100 K, and 1000 K, respectively. Note that these parameters may undergo further modification and optimization once the primary components have been determined. The neutronic calculation for the TFSCR core design was performed using the MCS code, a 3D continuous-energy Monte Carlo code developed at Ulsan National Institute of Science and Technology (UNIST) [18]. A library based on ENDF/B-VIII.0 was used in this study. During the simulation calculation process, the standard deviation for the k -value varied from 0.58 pcm to 1.28 pcm. Concurrently, the standard deviation for the pin power value ranged between 0.59% and 4.63%.

Table 4: Unit cell specifications.

Core parameter	Value
^{235}U enrichment (wt%)	10.00
Fuel tube inner radius (cm)	1.20
Fuel tube thickness (cm)	0.05715
TRISO packing fraction (%)	50.0
Coolant hole radius (cm)	1.50
Pin pitch (cm)	5.32

2.1. TRISO Fuel. The TFSCR concept utilizes TRISO particles as its fuel, which have exceptional structural integrity and fuel performance in high-temperature nuclear reactor designs. TRISO fuel particles are highly esteemed for their ability to endure challenging conditions, such as high temperature and high burnup, without any leakage of radioactive fission products. This is achieved by encapsulating each UO_2 particle within multiple coating layers, enabling them to withstand temperatures of up to 1600°C. Figure 2 illustrates the particle size and corresponding coating thickness obtained from reference [19] and utilized in this study.

2.2. Molten Salt Selection. Table 2 presents the fundamental physical parameters of three molten salts and water. The temperature of water is set at 300°C to reflect the typical coolant temperature in current PWRs. Additionally, a comparative temperature of 700°C is selected for better performance assessment of the salts. It is noteworthy that all candidate molten salts have melting points below 500°C and exhibit a volume expansion coefficient of only one-tenth that of water. This data indicates that molten salts

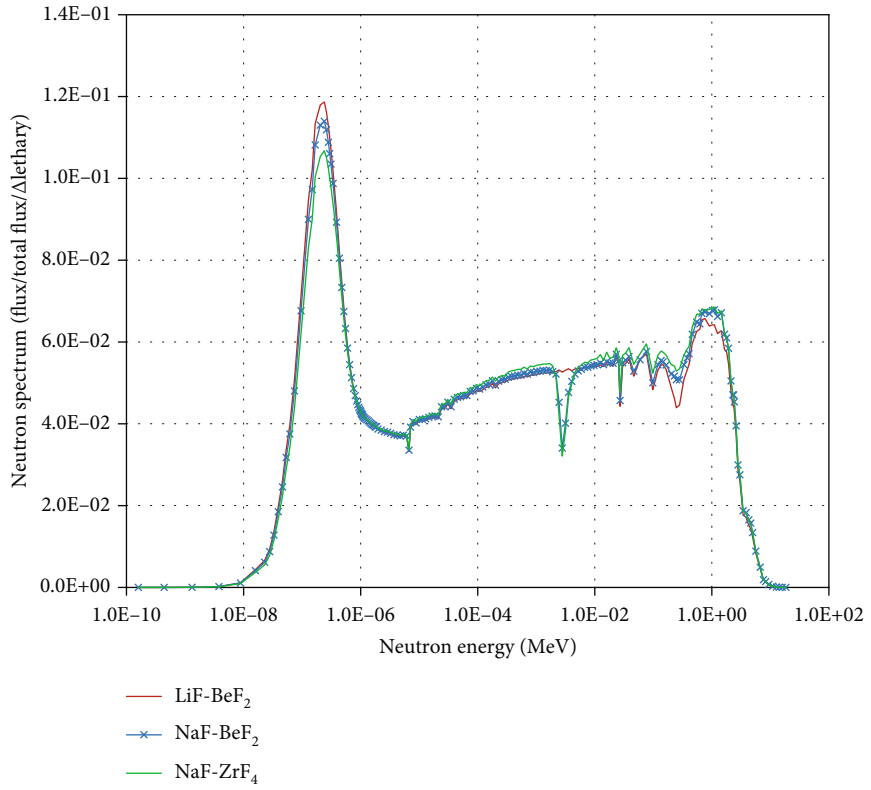

Figure 4: Neutron spectrum.

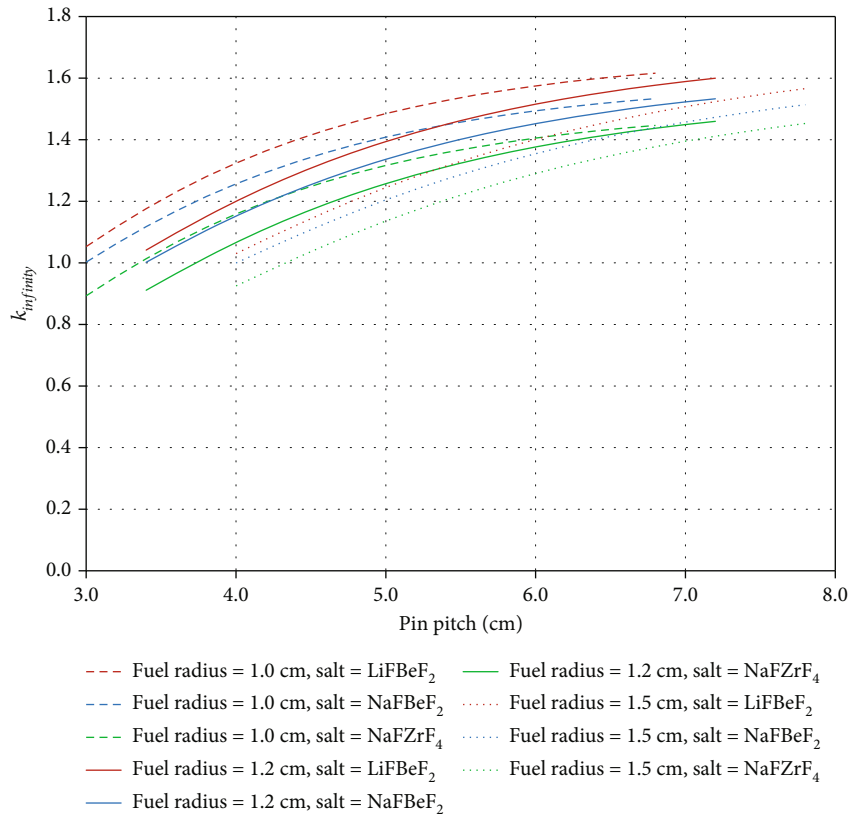

Figure 5: Variation of $\mathbf{k}_{\infty}$ value with moderator thickness.

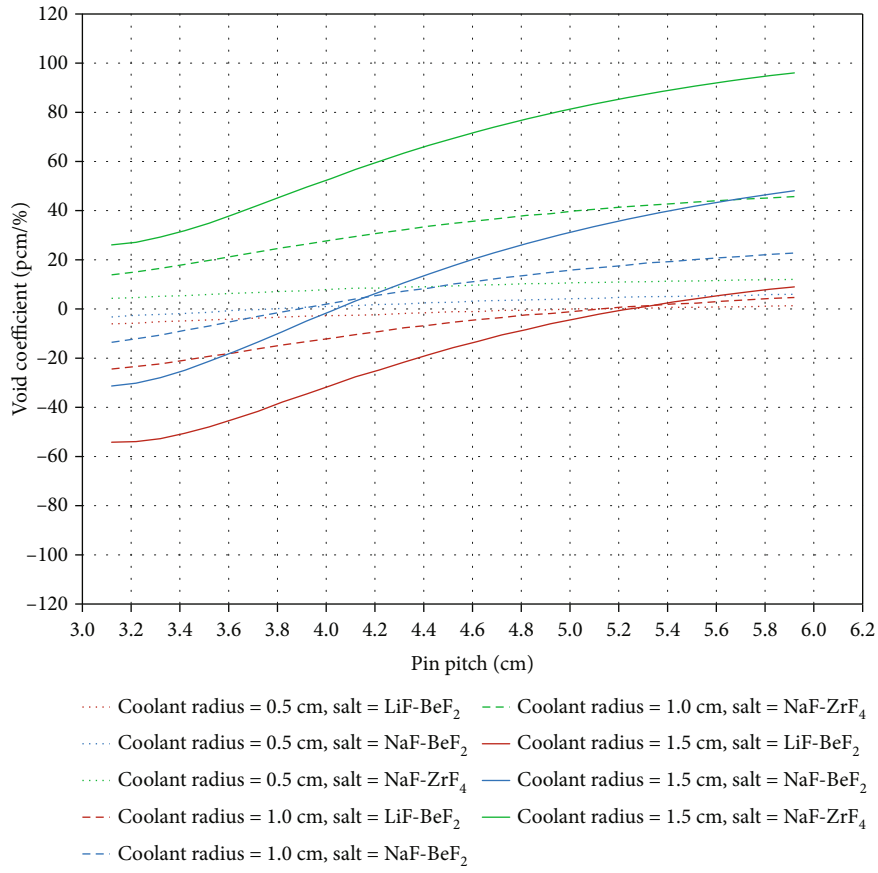

Figure 6: Void coefficients under various conditions.

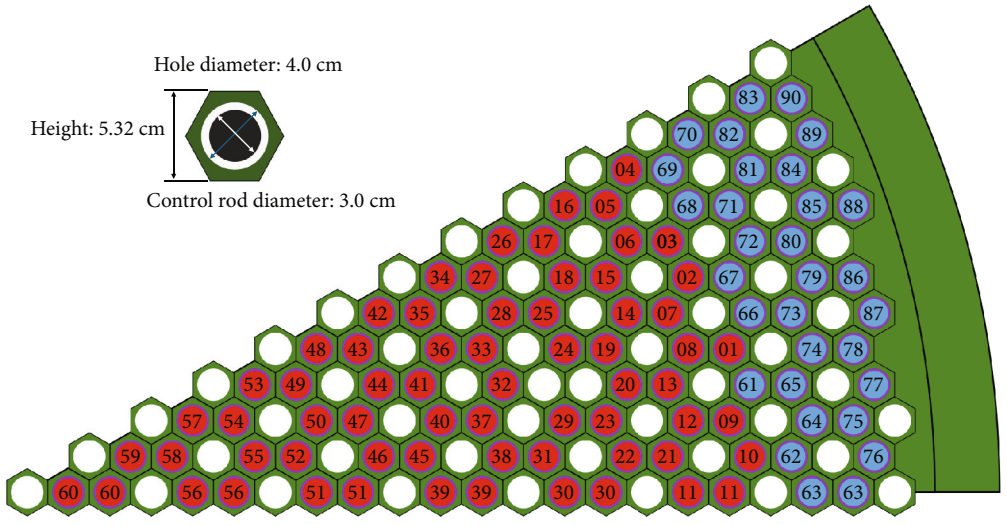

Figure 7: 1/12 core model.

experience minimal volume changes in response to temperature fluctuations, thereby resulting in negligible stress impacts on pipelines and structures. The viscosity of all salts is above 5 cP, and the viscosity value is more than 50 times that of water. Therefore, high viscosity should be considered during the design phase, necessitating the use of a larger diameter coolant hole to overcome the resistance caused by high viscosity [20]. The equations for the temperature dependency of the thermal properties in Table 2 are provided in reference 20.

In the absence of a tailored assessment system for molten salts, their performance can be evaluated from a general perspective. High thermal capacity and conductivity, as well as low viscosity and volume expansion coefficient, are key

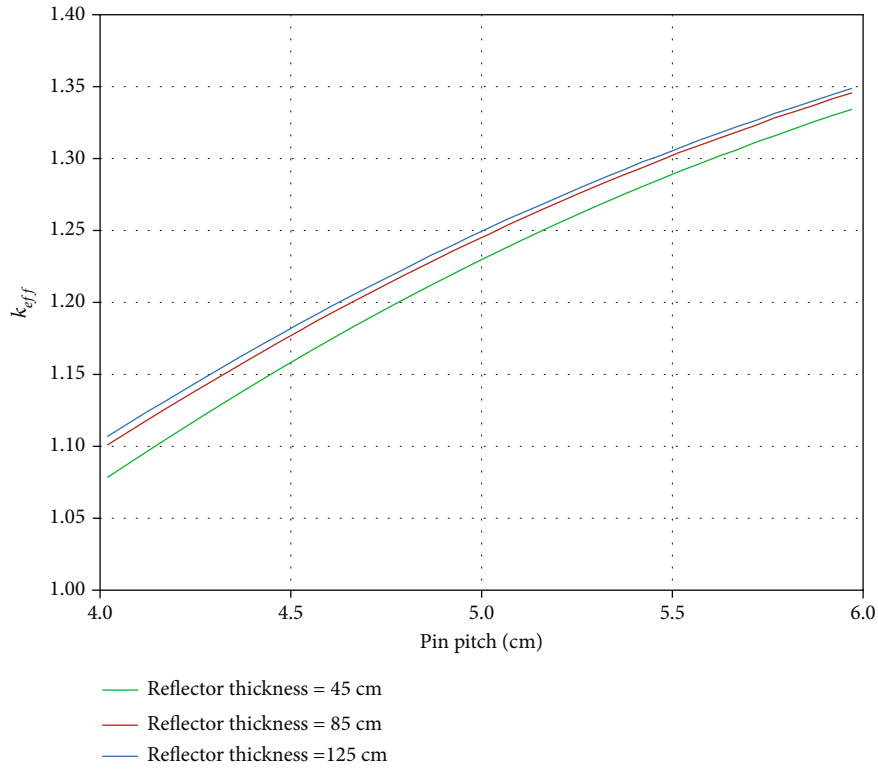

Figure 8: Influence of pin pitch and reflector thickness on $\mathbf{k_{eff}}$ value.

factors that determine their suitability. These characteristics can assist in ideal selection of molten salt. To assess the performance of molten salts as coolants, the coolant performance evaluation function (figure of merit (FOM)) developed by Bonilla [21] and Sanders [22] can be employed.

The formulas for the FOMs are as follows:

$$\begin{aligned}
\text{FOM (Turbulent forced convection)} &= \frac{\mu^{0.2}}{\left(\rho^2 C_p^{2.8}\right)},\\
\text{FOM (Heat exchanger area)} &= \frac{\mu^{0.2}}{\left(C_p^{0.6} k^{0.6} \rho^{0.3}\right)},\\
\text{FOM (Turbulent natural convection)} &= \left[\left(\frac{\mu^{0.2}}{\beta}\right)\rho^2 C_p^{1.8}\right]^{0.36},\\
\text{FOM (Laminar natural convection)} &= \left[\left(\frac{\mu}{\beta}\right)\rho^2 C_p\right]^{0.5},
\end{aligned} \tag{1}$$

where μ is the viscosity, ρ is the fluid density, C_p is the heat capacity, and β is the volume expansivity $= 1/\rho \cdot d\rho/dT$ (1/°C).

In most cooling scenarios, turbulent convection serves as the critical criterion for evaluation. The cooling capacity FOMs of water at 300°C and salts at 700°C are shown in Table 3. The lower the FOM value, the better the cooling capacity. After careful review, the molten salts LiF-BeF_2, NaF-BeF_2, and NaF-ZrF_4 have been identified as potential coolant candidates. Subsequent calculations will compare the nuclear properties of these candidate molten salts to determine the most suitable coolant.

Table 5: Core design parameters.

Core design parameters	Value
Thermal power (MWth)	100.0
Active core height (cm)	300.0
Effective core radius (cm)	115.0
Volumetric power density (W/cm^3)	8.02
Fuel power density (W/gU)	60.96
Control rod hole radius (cm)	2.00
Control rod radius (cm)	1.50
Total number of fuel channels	1080
Total number of coolant channels	547
Total number of control rods	12
Reflector thickness (cm)	85.0

2.3. Unit Cell Design. Figure 3 illustrates the unit cell model of the reactor core, showcasing the neutron moderator (green section), carrier (blue section), and coolant (white section). Both the carrier and the coolant are made of the same salt. The fuel tube is assumed to be zirconium alloy and is shown in purple, with 50% of the space filled with black-colored TRISO particles. Table 4 presents the unit cell parameters.

Table 6: Effect of control rod material on reactivity.

Material	Hot state (operation condition)		Cold state (300 K for all components)		
	k_{eff}	Reactivity ρ (pcm)	k_{eff}	Reactivity ρ (pcm)	SDM OSR[a] (pcm)
He	1.01336	+1,318	1.06639	+6226	—
B_4C	0.89635	-11,564	0.94342	-5998	-4557
Gd_2O_3	0.91920	-8,790	0.96985	-3108	-2112
AgInCd	0.91912	-8,800	0.97037	-3053	-2098
Hf	0.91636	-9,127	0.96665	-3450	-2438
Inconel slug	0.98897	-1,115	1.03571	+3448	+3674
SS304	0.99694	-307	1.04314	+4136	+4367

[a]Shutdown margin with one stuck rod.

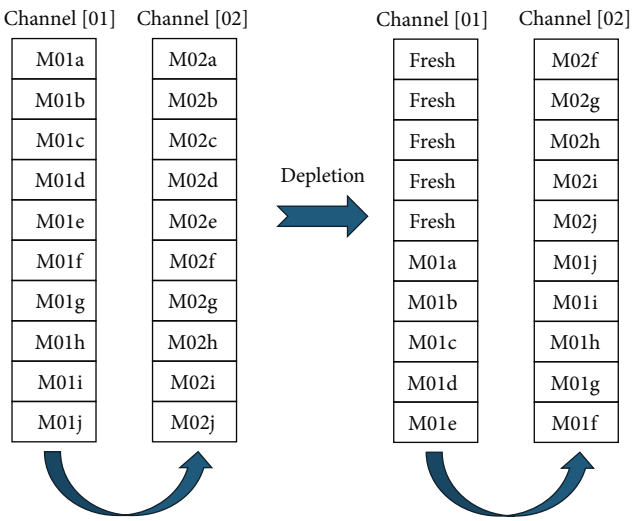

Figure 9: Fuel movement simulation.

Figure 4 showcases the neutron energy spectrum calculated using the proposed model for various molten salts. An enrichment of 99.995 wt% ^{7}Li was assumed in this calculation. Although there are minor differences in the neutron energy spectrum of the three molten salts, peaks are observed in the thermal neutron region for each, which is consistent with the neutron spectrum requirements of thermal reactors. Thus, an analysis based solely on the neutron spectra indicates that all three salts are suitable for use in a thermal reactor. The figure illustrates a notable dip in neutron spectra between 0.001 and 0.01 MeV for NaF-ZrF_4 and NaF-BeF_2 salts, which can be attributed to the influence of the large resonance of sodium (Na) element in that energy range.

The impact of pin pitch size variation on $\mathbf{k}_\infty$ was assessed for different inner radius (1.0 cm, 1.2 cm, and 1.5 cm) of the fuel tube conditions, and the corresponding results are presented in Figure 5. The calculation was conducted under the condition that all parameters except the tube inner radius and pin pitch remain constant. The findings demonstrate that $\mathbf{k}_\infty$ is influenced by both the fuel radius and pin pitch size variation, as well as the specific molten salt employed. Importantly, the results in Figure 5 reveal that the supercritical regime is readily achievable for all molten salts. Particularly noteworthy is the $\mathbf{k}_\infty$ curve for LiF-BeF_2, which surpasses that of other molten salts and aligns with neutron spectrum calculations. According to the calculation experience, the value of $\mathbf{k}_\infty$ must be greater than 1.3 to meet the requirements of subsequent design and analysis. Calculations indicate that the inner diameter of the fuel tube, ranging from 1.0 cm to 1.5 cm, meets this requirement. For subsequent designs, the inner diameter of the fuel tube will be 1.2 cm, although this may be adjusted in the future.

In reactors utilizing salt as a coolant, void formation in the core due to LOCA is unlikely since they operate at low pressure. However, coolant boiling can occur during operation due to factors such as blockages in the coolant channel, and the void coefficient needs to be considered. Figure 6 illustrates the void coefficients under different conditions with a fuel radius of 1.2 cm. The void coefficients were evaluated assuming complete voiding at 100%. The void coefficient increases as the pin pitch value increases. The physical interpretation for this phenomenon is as follows: The coolant salt acts as both a moderator and a weak absorber because the absorption cross-section of the salt is much larger than that of the graphite moderator. When the pin pitch is small, the role of salt as a moderator is relatively more important than that as an absorber because the amount of graphite moderator is small, and the absence of the coolant salt results in a decrease in reactivity. On the other hand, when the pin pitch is large, the role of salt as an absorber is relatively more important than that as a moderator because the amount of graphite moderator is large, and the absence of the coolant salt results in the increase of the reactivity. However, a comprehensive analysis demonstrates that selecting LiF-BeF_2 as the coolant not only satisfies the requirement for a negative void coefficient but also achieves the maximum $\mathbf{k}_\infty$ value. Consequently, considering the overall reactor performance, LiF-BeF_2 is undoubtedly the optimal choice. This choice aligns with the utilization of LiF-BeF_2 as the molten salt in numerous MSR design schemes.

Additionally, calculations indicate that as the coolant radius increases, both the coolant volume and its neutron absorption capacity also increase. Similarly, the neutron absorption capacity of the moderator increases with the

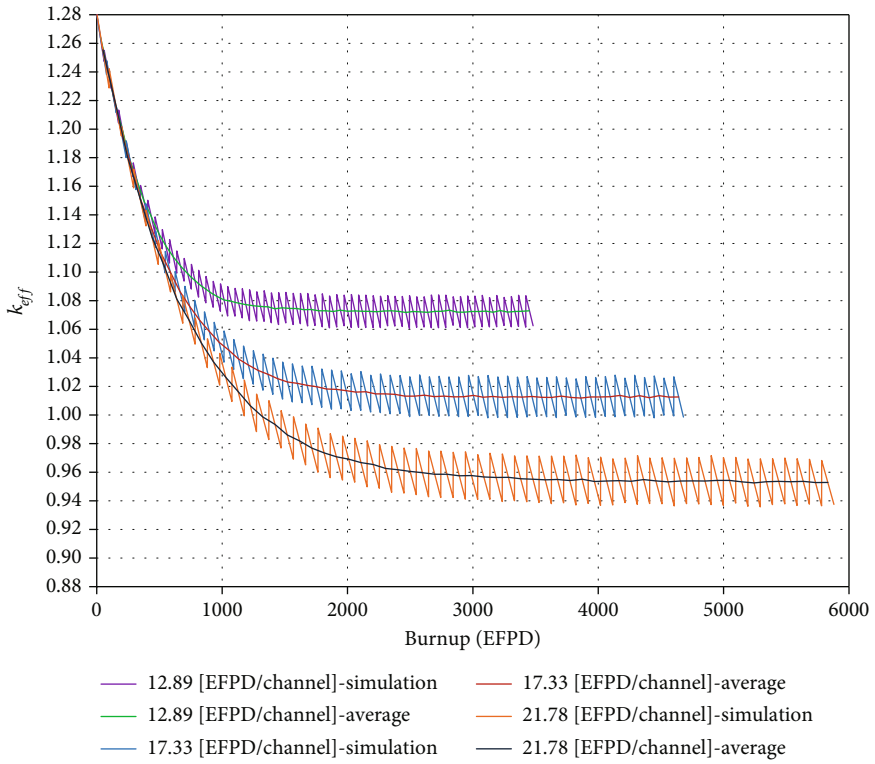

Figure 10: Core burnup calculation.

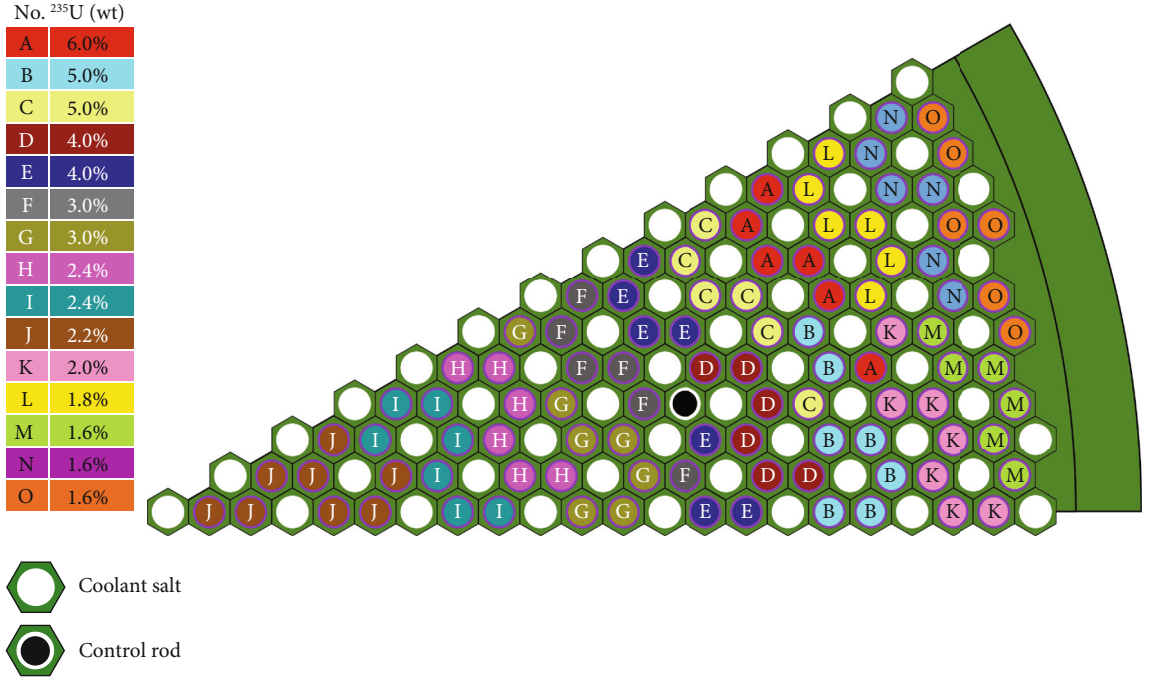

Figure 11: Initial fuel loading method.

volume of the moderator. As a result, in the event of coolant loss, a larger coolant radius results in a more significant shift in the void coefficient. Based on these findings, a recommended coolant radius of 1.5 cm has been determined.

2.4. Core Design. Figure 7 illustrates the 1/12 core model with green regions for moderator and reflector, white regions for coolant, and blue and red regions for fuel. Red and blue indicate areas where the fuel is relatively less burnt and more burnt, respectively. The numbers indicate the

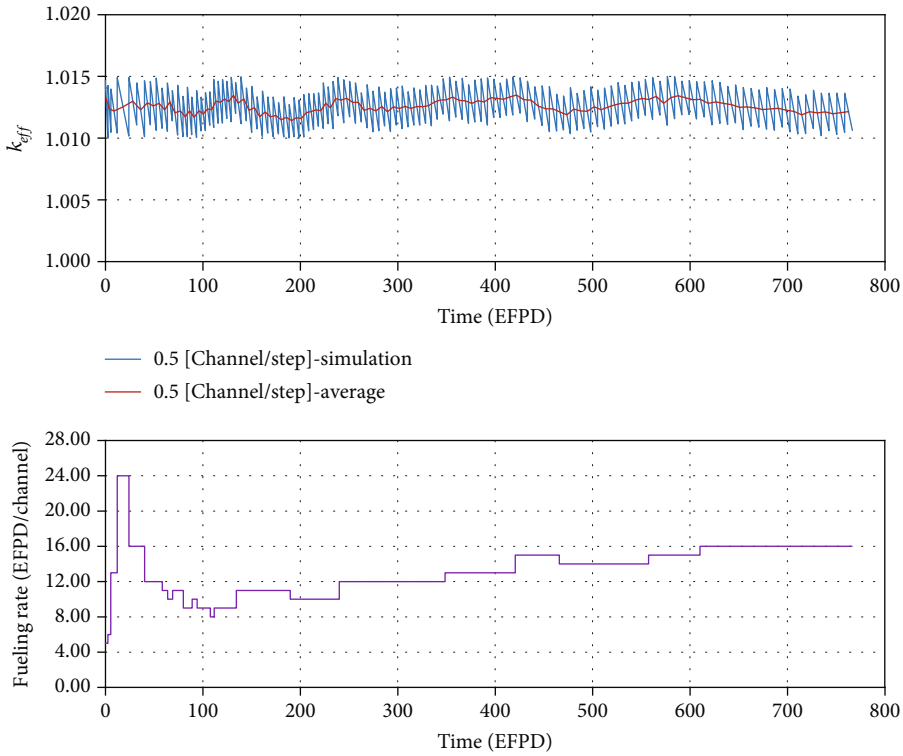

Figure 12: Core burnup simulation results.

Table 7: Fuel burnup parameters of the core.

Parameters	Value
Fueling rate at equilibrium state (EFPD/channel)	16.0
Mass fueling rate at equilibrium state (kgU/EFPD)	1.14
Discharge burnup at equilibrium state (MWD/kgU)	87.78

pathway that the fuel follows. Fresh TRISO fuel is delivered via channel "01" as illustrated in Figure 7. It follows the designated pathway indicated by the channel numbers, before being discharged through channel "90" also shown in Figure 7. The fuel moves inward and then outward past the core center to form a low-leakage core. The reflector, made of graphite, shares the same material as the moderator. The core is divided into 12 regions at an angle of 30 degrees to ensure mirror symmetry. The active core height is 300 cm with an effective core radius of 115 cm. Based on a thermal power of 100 MWth, calculations indicate a total of 1080 fuel channels within the core, with an average fuel power density of 60.96 W/gU and a volumetric power density of 8.02 W/cm^3. To investigate the influence of the core reflector thickness and pin pitch on the core $\mathbf{k_{eff}}$ values, calculations were performed for various pin pitch values.

Figure 8 shows the $\mathbf{k_{eff}}$ value as a function of pin pitch and reflector thickness. The analysis shows that both an increase in the thickness of the reflector and an increase in the pitch of the pin correspond to an increase in the value of $\mathbf{k_{eff}}$. Furthermore, Figure 6 demonstrates that the void coefficient also rises with increasing pitch values; however, for this design, a negative void coefficient is required. Ultimately, considering both Figures 6 and 8, a pin pitch of 5.32 cm and reflector thickness of 85 cm were determined. Table 5 presents the summary of core design parameters.

In this design, fuel can be supplied online, allowing reactivity to be controlled by adjusting the fueling rate. This method is consistent with the approach used in liquid fuel reactors to control reactivity. Shutdown can be achieved by ceasing fueling. However, in the case of a rapid shutdown requirement, control rods can be utilized to ensure safety. The effect of control rod positions on reactivity was investigated, and the control rod position with the most significant effect on reactivity is indicated as "CR" in Figure 7. When the control rods are out, the control rod channels are filled with helium. The control rod channel has a diameter of 4 cm, and the control rod diameter is 3 cm. Table 6 presents the results of calculations for various control rod materials and evaluates the effect of a single control rod failure on the $\mathbf{k_{eff}}$ value. It was observed that the B_4C control rod had the largest impact on reactivity, while Gd_2O_3, AgInCd, and Hf also satisfied the shutdown requirement. Hence, B_4C was temporarily selected as the control rod material.

2.5. Core Burnup Calculation. Figure 9 depicts a schematic diagram that illustrates the simulation of fuel distribution and movement within the reactor. During actual operations, TRISO fuel particles are conveyed through the pipes by the carrier molten salt, both moving at the same speed, thereafter referred to as the "fueling rate." To simulate this process, the fuel is divided equally into ten blocks along the z-axis. The fuel is incrementally introduced into the pipeline for each burnup step during the simulation, with half a channel

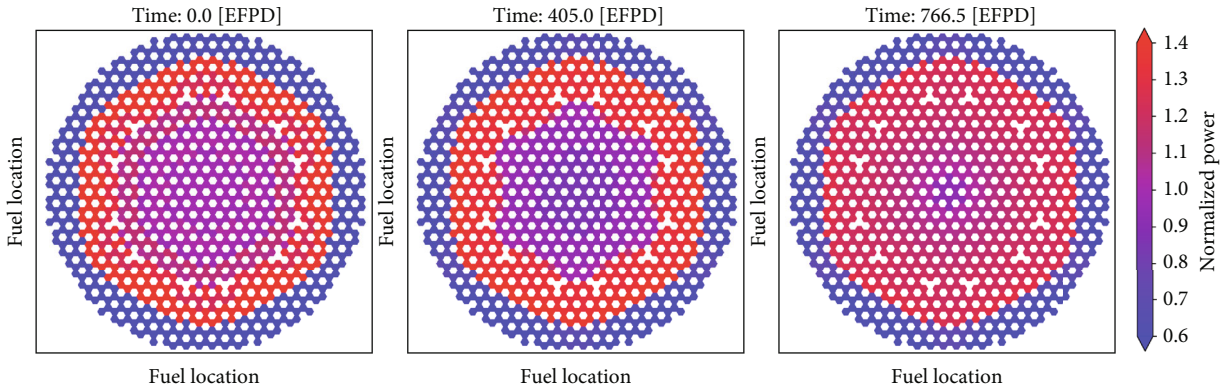

Figure 13: Core power distribution during operation.

Table 8: Temperature and void coefficients of the core.

Coefficients of reactivity	Value
Isothermal temperature coefficient at fresh state (pcm/K)	-4.398
Fuel temperature coefficient at fresh state (pcm/K)	-2.263
Moderator temperature coefficient at fresh state (pcm/K)	-2.295
Coolant temperature coefficient at fresh state (pcm/K)	-0.435
Coolant void coefficient at fresh state (pcm/%void)	-8.77
Carrier void coefficient at fresh state (pcm/%void)	-4.35
Isothermal temperature coefficient at equilibrium state (pcm/K)	-8.525
Fuel temperature coefficient at equilibrium state (pcm/K)	-2.785
Moderator temperature coefficient at equilibrium state (pcm/K)	-1.935
Coolant temperature coefficient at equilibrium state (pcm/K)	-0.205
Coolant void coefficient at equilibrium state (pcm/%void)	-27.23
Carrier void coefficient at equilibrium state (pcm/%void)	-15.59

being refueled at each burnup step. This approach mitigates errors arising from repetitive burning of fuel at the same axial location when a full channel is refueled at each burnup step. Figure 9 illustrates the fuel movement in the first two channels between burnup steps.

Figure 10 illustrates the effective multiplication factor for different fueling rates. Three different fueling rates are considered, and the design requirements are satisfied when the fueling rate is 17.33 effective full power days (EFPDs) per channel. The burnup curve eventually reaches equilibrium state with increasing simulation time. Furthermore, maintaining a reactivity margin within the range of 1000 pcm to 1500 pcm at an equilibrium state can be employed for future core analyses. As fuel depletion progresses, the final $\mathbf{k_{eff}}$ value is saturated, indicating that the design meets the requirements for online refueling. However, during the beginning of the life (BOL) stage, a large value of $\mathbf{k_{eff}}$ is observed. To address this problem, adjustments to the initial fuel loading are necessary in order to rapidly converge the $\mathbf{k_{eff}}$ value to an equilibrium state.

To determine the initial fuel loading pattern for the core, the fuel is divided into 15 regions, as shown in Figure 11. Fuel enrichment zoning is adopted for moderate radial power distribution and initial reactivity. At the same time, low-leakage core design is considered, and the outer side of the fuel inlet is designed as low-enrichment fuel. The method ensures that the reactor can quickly reach the equilibrium state during the burnup calculation. The zones listed in the table correspond to the fuel positions shown in the figure, specifying the ^{235}U enrichment in the initial fuel loaded into each zone. With this loading method, a calculated $\mathbf{k_{eff}}$ value of 1.01467 is obtained, initially.

Figure 12 displays the recalculated core fuel depletion results obtained using the new loading method. It is assumed that all the control rods are out during the simulation. The figure also illustrates the corresponding fueling rate during the depletion process. In the simulation, a standard unit of fuel (half channel) is added at each step, and the speed is regulated by adjusting the time interval of depletion. The simulation calculations demonstrate that the system reached an equilibrium state after about 600 effective full power days of operation. These results indicate that the current parameters satisfactorily meet the preliminary design requirements. Table 7 shows the fuel burnup parameters of the core.

Figure 13 illustrates the power distribution of fuel within the reactor core. The colors in the figure represent the normalized power. Red indicates higher values, blue indicates lower values, and purple represents transition zones. The

power distribution pattern reveals that the maximum power is concentrated at the inlet of the core fuel, while the minimum power is observed at the outlet.

In practice, it is essential to consider variations in the packing fraction of the TRISO particles due to temperature changes, which can lead to variations in the volume of the molten salt and subsequent impact on reactivity. The rate of volume expansion for LiF-BeF_2 with respect to temperature is approximately 2.52×10^{-4} (1/°C) [20]. Therefore, it is necessary to consider the effect of these volume variations on the core temperature coefficient, the fuel temperature coefficient, and the isothermal temperature coefficient. Considering the effects of temperature change and volume expansion, the variation of the temperature coefficient is calculated. In reactors utilizing salt as a coolant, void formation in the core due to LOCA is unlikely since they operate at low pressure. However, coolant boiling can occur during operation due to factors such as blockages in the coolant channel, and the void coefficient needs to be considered. For void coefficient calculation, a 100% complete voiding was assumed. Table 8 shows the temperature coefficients and the void coefficients of the core.

3. Conclusions

This paper presents an innovative design of a molten salt-cooled reactor that utilizes TRISO fuel and operates in high-temperature environments. The use of dedicated pipelines allows for the transportation of TRISO fuel particles, enabling a continuous and stable fuel supply. By adjusting the fueling rate, a continuous operation of the reactor with online refueling can be achieved. The use of TRISO fuel addresses the radiation contamination concerns associated with liquid fuel in MSRs while retaining the benefits of online refueling in MSRs. Moreover, it maintains fuel circulation inside the core through the fuel tube during operation, avoiding the radiation exposure issue arising from the recycling of pebbles and the uncertainty issue arising from the stochastic core composition. This approach optimizes the safety, economics, and adaptability of the reactor.

In conclusion, this design integrates the advantages of TRISO fuel and molten salt cooling, providing a secure, efficient, and sustainable solution for molten salt-cooled reactors. By utilizing the exceptional properties of TRISO fuel, such as its high-temperature resistance and ability to contain radioactive materials, in conjunction with molten salt coolant, this design ensures improved safety and operational efficiency. It represents a promising approach towards the development of advanced molten salt-cooled reactors.

The feasibility of this design concept has been verified from a nuclear design standpoint, but further optimization is needed to enhance the reactor's overall performance and efficiency. It is also necessary to conduct sensitivity analysis on parameters according to specific requirements and conduct thermal analysis on the core at the same time and use the analysis results to adjust the design parameters of the core again.

Data Availability

The data used to support the findings of this study are included within the article.

Conflicts of Interest

The authors declare that they have no conflicts of interest.

Acknowledgments

This work was supported partly by the National Research Foundation of Korea (NRF) grant funded by the Korea government (MSIT) (no. 2019R1A2C2089962) and partly by the Korea Institute of Energy Technology Evaluation and Planning (KETEP) and the Ministry of Trade, Industry & Energy (MOTIE) of the Republic of Korea (no. 20214000000410).

References

[1] J. Serp, M. Allibert, O. Beneš et al., "The molten salt reactor (MSR) in generation IV: overview and perspectives," *Progress in Nuclear Energy*, vol. 77, pp. 308–319, 2014.

[2] D. E. Holcomb, G. F. Flanagan, G. T. Mays, W. D. Pointer, K. R. Robb, and G. L. Yoder Jr., *Fluoride salt-cooled high-temperature reactor technology development and demonstration roadmap*, ORNL/TM-2013/401, Oak Ridge National Lab. (ORNL), 2013.

[3] B. M. Elsheikh, "Safety assessment of molten salt reactors in comparison with light water reactors," *Journal of Radiation Research and Applied Sciences*, vol. 6, no. 2, pp. 63–70, 2013.

[4] APR1400-K-X-FS-14002-NP, *AP1400 Design Control Document Tier 2, Chapter 3*, Korea Electric Power Corporation and Korea Hydro & Nuclear Power (KEPCO & KHNP), 2014.

[5] A. Sowder, S. Krahn, B. Burkhardt, T. Ault, and A. Croff, *Program on technology innovation: technology assessment of a molten salt reactor design: the liquid-fluoride thorium reactor (LFTR)*, 2015 Technical Report 3002005460, Electric Power Research Institute (EPRI), 2015.

[6] K. Furukawa, *Status of Small Reactor Designs Without On-Site Refueling, IAEA-TECDOC-1536*, pp. 821–856, International Atomic Energy Agency (IAEA), 2007.

[7] T. Schønfeldt and E. Klinkby, "Molten salt thermal wasteburner," in *Molten salt reactors and thorium energy*, pp. 609–618, Woodhead Publishing, 2017.

[8] V. K. Varma, D. E. Holcomb, F. J. Peretz et al., *AHTR mechanical, structural, and neutronic preconceptual design*, ORNL/TM-2012/320, Oak Ridge National Lab. (ORNL), 2012.

[9] R. Greene Sherrell, C. Gehin Jess, H. D. Eugene et al., *Pre-conceptual design of a small modular fluoride salt-cooled high temperature reactor (SmAHTR)*, ORNL/TM-2010/199, Oak Ridge National Lab. (ORNL), 2011.

[10] C. Andreades, A. T. Cisneros, J. K. Choi et al., "Design summary of the Mark-I pebble-bed, fluoride salt–cooled, high-temperature reactor commercial power plant," *Nuclear Technology*, vol. 195, no. 3, pp. 223–238, 2016.

[11] M. Margulis and E. Shwageraus, "Advanced gas-cooled reactors technology for enabling molten- salt reactors design–optimisation of a new system," *Nuclear Engineering and Design*, vol. 385, article 111546, 2021.

[12] P. A. Demkowicz, *TRISO Fuel Part II Accident Performance and NRC Engagement*, INL/MIS-21-62430-Rev000, Idaho National Lab. (INL), 2021.

[13] J. D. Stempien, J. D. Hunn, R. N. Morris, T. J. Gerczak, and P. A. Demkowicz, *AGR-2 TRISO Fuel Post Irradiation Examination Final Report*, INL/EXT-21-64279-Rev000, Idaho National Lab. (INL), 2021.

[14] M. Holbrook, *Review and assessment of NGNP PIRTs for TRISO and HTGR technologies*, INL/RPT-23-72036-Rev000, Idaho National Laboratory (INL), 2023.

[15] T. Haynes, A. Battistini, A. Leide et al., "Peridynamic modelling of cracking in TRISO particles for high temperature reactors," *Journal of Nuclear Materials*, vol. 576, article 154283, 2023.

[16] H. Wei, J. Zhang, X. Jian et al., "Effects of the mesostructures and irradiation conditions on the thermo-mechanical coupling behaviors in LWR-used fully ceramic-microencapsulated fuel pellets," *Nuclear Materials and Energy*, vol. 34, article 101387, 2023.

[17] S. Torquato, T. M. Truskett, and P. G. Debenedetti, "Is random close packing of spheres well defined?," *Physical Review Letters*, vol. 84, no. 10, pp. 2064–2067, 2000.

[18] H. Lee, W. Kim, P. Zhang, A. Khassenov, Y. Jo, and D. Lee, "Development status of Monte Carlo code at UNIST," in *Proceedings of the Korean Nuclear Society Spring Meeting*, Korean Nuclear Society, Jeju, 2016.

[19] Y. M. Kim, C. K. Jo, and E. S. Kim, "Optimum coating layer thicknesses of a TRISO having an 800-μm UO2 kernel under normal operation conditions of a 10-MWth block-type HTGR," *Nuclear Engineering and Design*, vol. 381, article 111332, 2021.

[20] D. F. Williams, L. M. Toth, and K. T. Clarno, *Assessment of candidate molten salt coolants for the advanced high-temperature reactor (AHTR)*, ORNL/TM-2006/12, Oak Ridge National Lab. (ORNL), 2006.

[21] C. F. Bonilla, "Comparison of Coolants," in *Nuclear Engineering Handbook, Sect. 9-3, Chap. 6.5*, H. Etherington, Ed., pp. 9–90, 1958.

[22] J. P. Sanders, *A Review of Possible Choices for Secondary Coolants for Molten Salt Reactors*, Oak Ridge National Laboratory, Oak Ridge, TN, USA, 1971.